

Low-cost nebulizer spray deposited conduction mechanism of thin film ZnO nanoparticles

B. Amudhavalli^a, R. Mariappan^b, M. Prasath^{a,*}

^a*Department of Physics, Periyar University PG Extension Centre, Dharmapuri-636 705, Tamilnadu, India*

^b*Department of Physics, Adhiyamaan College of Engineering, Hosur, Krishnagiri-635109, Tamilnadu, India*

The Zinc Oxide (ZnO) thin films have been deposited on glass substrate at different temperature from 300 to 500 °C by nebulizer spray pyrolysis technique. The prepared films were characterized by X-Ray diffraction (XRD), High resolution scanning electron microscope (HRSEM), Energy dispersive analysis by X-rays (EDAX), Photoluminescence (PL), UV-Vis-NIR spectrometer and impedance spectroscopy, respectively. The XRD confirms that the films are polycrystalline in nature with hexagonal wurtzite crystal structure with (002) plane as preferential orientation. The various parameters such as crystallite size, micro strain, and dislocation density were calculated from X-ray diffraction. HR-SEM images show smooth, tiny grains and dense morphology. The PL studies exhibits two emission peaks one at 389 nm corresponding to band gap excitonic emission and another located at 490 nm due to the presence of singly ionized oxygen vacancies. The UV-Vis-NIR spectrometer confirms the possibility of good transparent ZnO films with an average transmission of about ~85-95% in the visible region and optical band gap shifted from 3.37 eV to 3.2 eV with increase in temperature and which is supported by PL study. The semiconductor behaviour and activation energy of these films have been confirmed by impedance spectroscopy measurements.

(Received September 23, 2022; Accepted January 13, 2023)

Keywords: X-ray diffraction, Surface morphology, Optical; Electrical properties, Activation energy

1. Introduction

In recent years, zinc oxide materials have been carried out to modified the properties for different applications such as solar cells, gas sensor, surface acoustic wave device, varistors, transparent conducting electrodes and also in a wide variety of electronic applications [1-3]. Zinc oxide thin films have attracted much attention due to their valuable properties such as high optical transparency in the visible region, high thermal stability, low electrical resistivity and absence of toxicity. It is wide band gap semiconductor with a band gap value varied from 3 to 3.5 eV [4]. However, very easy to dopants can make it n-type semiconductor.

Zinc oxide thin films have been prepared by various methods, such as nebulizer spray method [5-7], chemical vapor deposition [8,9], chemical bath deposition [10,11], sol-gel [12,13], thermal evaporation [14,15], sputtering [16,17] and pulsed laser deposition [18,19] have been deposited for the production of ZnO films. Nebulizer spray pyrolysis techniques has received a little bit of more advantages due to their better homogeneity, stoichiometry control, low cost effectiveness, low processing temperature, simplicity and easier deposition of large area films, and compared to other methods, which allow the possibility of prepared films with the required properties for various applications.

In this work, the ZnO thin films were prepared by nebulizer spray pyrolysis technique using a 0.1 M of zinc acetate was dissolved in deionized water mixed with methanol in the ratio of

* Corresponding author: sanprasath2006@gmail.com
<https://doi.org/10.15251/JOR.2023.191.53>

1:3 and different temperature from 300 to 500 °C. The structural, electrical, surface morphological and optical properties of ZnO films have been carried out.

2. Experimental details

The ZnO thin films were chemical used for analytical reagent grade (98.9% purity procured from sigma Aldrich). The ZnO film films were deposited at different temperatures from 300 to 500 °C in steps of 50 °C through nebulizer spray pyrolysis technique. 0.1 M zinc acetate dehydrate was dissolved in 25 ml of de-ionized water mixed with methanol in the ratio of 1:3 and stirred for 10 min using magnetic stirrer until the pH value reached 7. Fig. 1 shows the schematic diagram of the NSP setup. First, connect one end of the tubing to the air outlet on the compressor and the other end into the bottom of the prepared solution cup. When the solution is deposited in as an aerosol, it is easily deposited into the glass plates. The nebulizer machine works very similar to an deposition but delivers the machine at a slower rate. Confirm the machine is turned off before unscrewing the cup and filling it with the prescribed amount of solution. Put the cup's top back on after filling it with machine. The prepared solution was sprayed onto the ultrasonically cleaned glass substrates and substrate temperature varied from 300 to 500 °C and controlled within ± 5 °C by using Iron-Constantan thermocouple kept on the metallic hot plate surface. The solution flow was added to the pressurized air at a constant pressure of 30 Pa. The nozzle to substrate distance was 5 cm and the time for the film deposition was about 10 min.

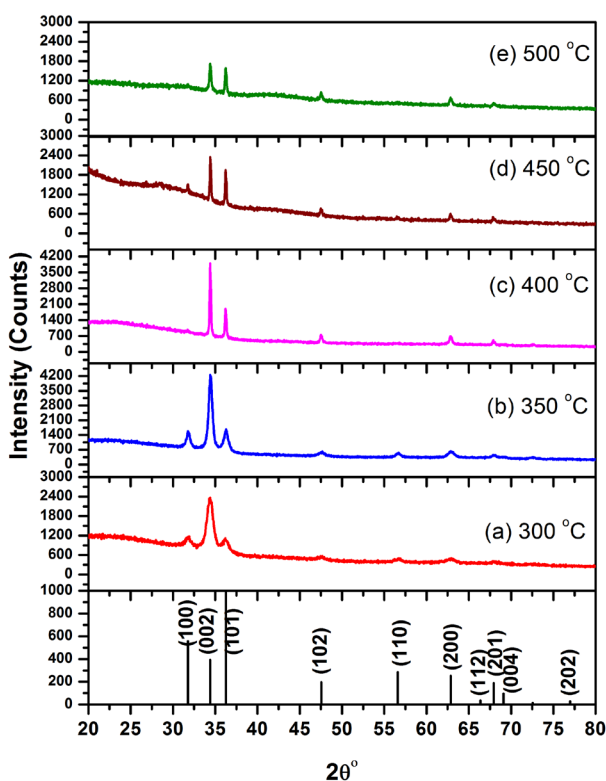


Fig. 1. XRD patterns of sprayed ZnO thin films.

Powder X-ray diffraction (XRD, Bruker D8 advanced diffractometer) measurements using CuK α radiation ($\lambda = 0.154$ nm) were employed to identify the crystalline phase of the prepared material. Surface morphology and compositional analysis of ZnO thin films were carried out using a high resolution scanning electron microscope and energy dispersive X-ray analysis setup (EDAX) which is attached with HRSEM (FEI QuantaFEG 200), respectively. Impedance

measurements were done using a Frequency Response, Solartron, Model 1360 coupled with the Solartron Dielectric Interface, 1296. The room temperature photoluminescence spectrum was performed on a spectrofluorimeter (fluorolog model FL3-11). The optical studies of the films were done with a UV-Vis-NIR spectrophotometer (Model JASCO-V-570) in the range from 300 to 2500 nm.

3. Results and discussion

3.1. XRD analysis

XRD analysis there is no phase transformation during the different temperature, the main transformations are recovery, recrystallization, and grain growth. The XRD patterns of the deposited ZnO thin films were deposited at different temperature from 300 to 500 °C are shown in Fig. 1a-e. The deposited ZnO thin films reveals that the polycrystalline in nature with wurtzite hexagonal crystal structure as preferential orientation along (002) plane and it is compared with standard JCPDS No. 01-080-0074. The diffraction peaks were observed for 2θ values 31.7°, 34.4°, 36.3°, 47.6°, 56.6°, 62.8°, and 68.0°, corresponds to (100), (002), (101), (102), (110), (103) and (112) planes. On comparison of peak intensities for indexed planes (100), (002) and (101). It is observed that the peak intensity for (002) remained constant, while that for (100) and (101) got decreased with increase in temperature from 300 to 500°C. These changes in the peak intensity suggest the changes the leaf nanostructures to spherical nanostructures. The lattice constants, crystalline sizes, dislocation density, microstrain were calculated by the XRD pattern data [20-23] as listed in Table 1.

The lattice parameters 'a' & 'c', were calculated using following Equation (1)

$$\frac{1}{d^2} = \frac{4}{3} \left[\frac{a^2 + hk + k^2}{a^2} \right] + \frac{l^2}{c^2} \quad (1)$$

The crystalline size (D) was calculated using following Equation (2)

$$D = \frac{K\lambda}{\beta \cos\theta} \quad (2)$$

The dislocation density (δ) was calculated using following Equation (3)

$$\delta = \frac{1}{D^2} \quad (3)$$

The micro strain (ϵ) was calculated using following equation (4)

$$\epsilon = \frac{\lambda}{D \sin\theta} - \frac{\beta}{\tan\theta} \quad (4)$$

The variation of crystalline size, dislocation density and microstrain with temperature for ZnO thin films are shown in Fig. 2. As the temperature increases from 300 to 500°C (Fig. 2), the grain sizes growth is the main microstructural change in the samples, which leads to a decrease in the mechanical characteristics of this ZnO films. The average crystalline size value for ZnO films was found to be increased from 22 nm to 62 nm with increase in temperature. It is seen from the Fig.2, a increase in crystalline size values with an increase in temperature is attributed to the enlargement of grain sizes and a decrease in the micro strain while increase in dislocation density.

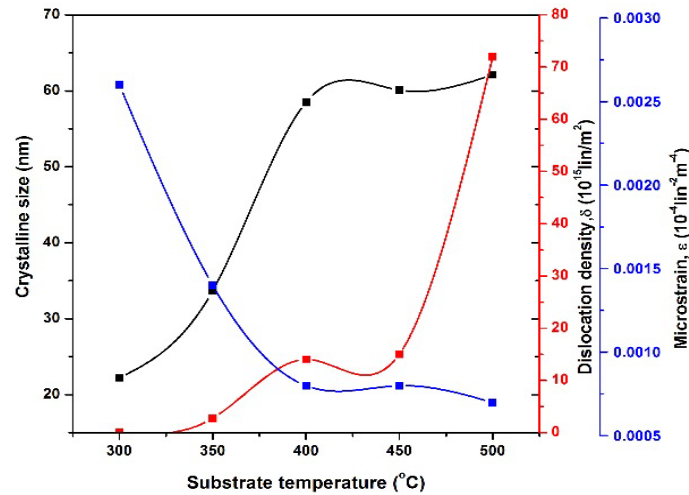


Fig. 2. Variations of crystallite size, dislocation density, micro strain with substrate temperature for ZnO thin films.

3.2. Surface morphological analysis

The surface morphology and compositional analysis of the ZnO thin films at different temperatures from 300 to 500 °C were examined by HR-SEM attached with EDAX spectrum are shown in Fig. 3a-e. It is seen from Fig.3a & b, the grains are growth over the substrate with uniform, very well-boundary and vertically growth nano-leaf like structures. The average length of grain sizes was found to be ~40-60 nm. As increased in temperatures from 400 to 450°C, we observed that the Fig.3c & d, the grains are changed to clusters composed of multiple grains with sharp edges, showing upon the surface and it is found to be ~65 nm for 450°C. As deposited at 500°C, the clusters tend to merge, forming a more compact and non-uniform, but highly dense and irregular shape in grains.

The compositional analysis of ZnO thin films were carried out by the energy dispersive analysis by X-rays (EDAX) at difference temperature are shown in Fig.3a-e. It is seen from Fig.3a-e, the all deposited ZnO films are confirmed the presence of Zn and O elements and atomic percentage of ZnO nanoparticles nearer stoichiometry at 400 °C. The presence of the silicon peak in the spectra is due to the glass substrate component.

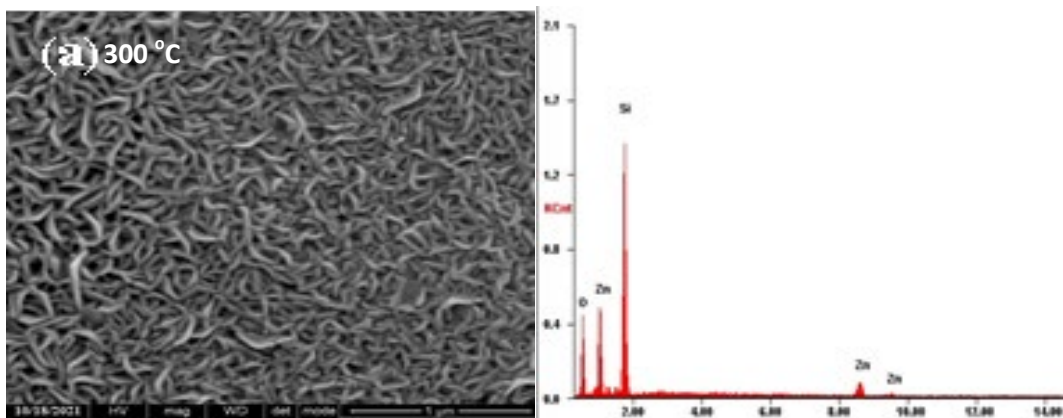


Fig. 3.1 High resolution SEM images and EDAX spectra of sprayed ZnO thin films.

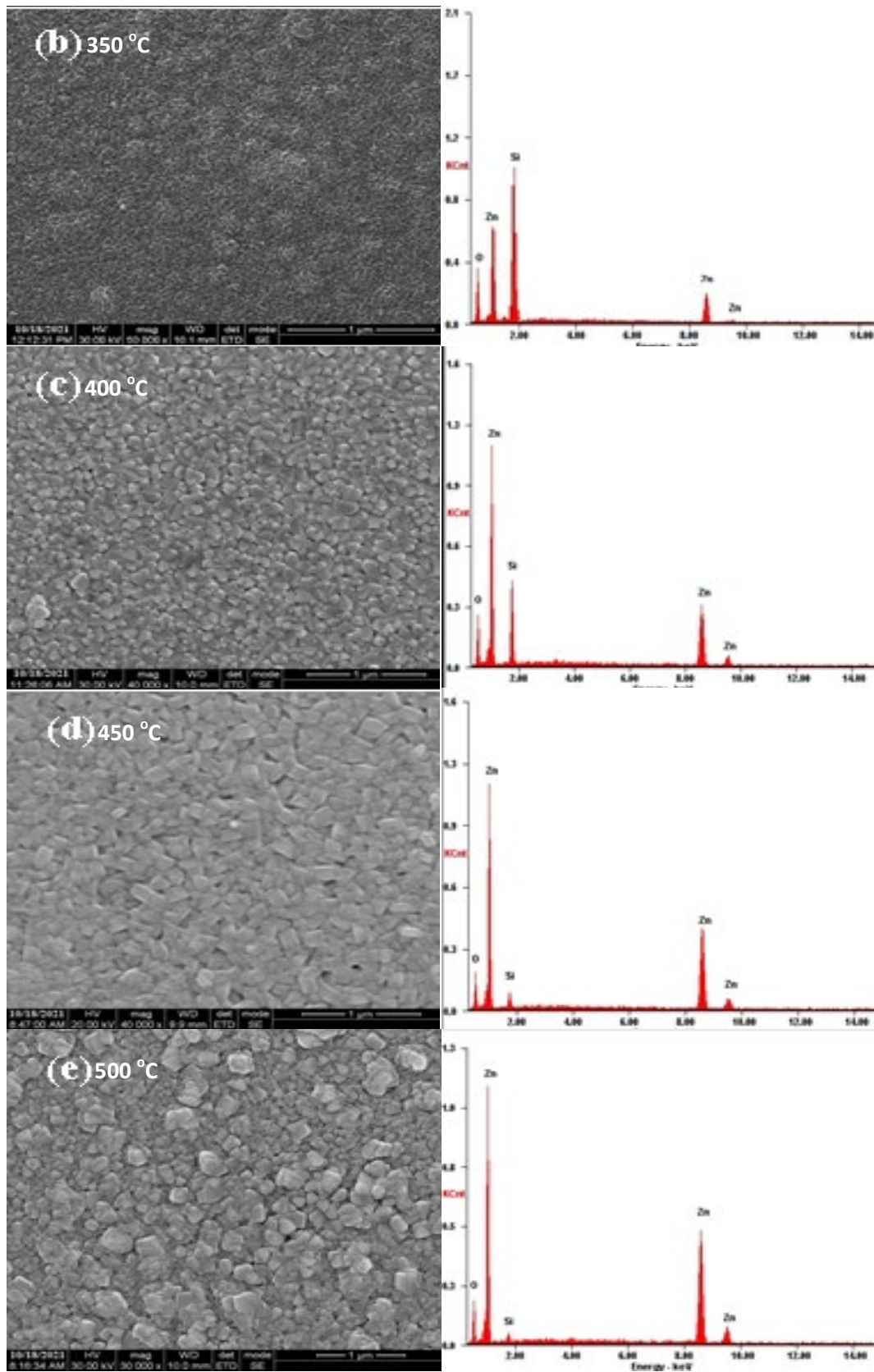


Fig. 3.2 High resolution SEM images and EDAX spectra of sprayed ZnO thin films.

3.3. Photoluminescence analysis

The photoluminescence (PL) spectra of sprayed ZnO thin films were deposited at different temperature, 300, 350, 400 and 500 °C with excitation wavelength of 321 nm are shown in Fig.4a-d. Wide green emission of ZnO was ascribed to oxygen impurities, which existed both on the inside and on the surface of the ZnO nanoparticles [24-26]. Surface defects, which existed only on the surface of emission material, decreased photoluminescence intensity because the surface defect level increased the nonradiative transitions [27-29]. Therefore, the photoluminescence intensity of the nanoparticles, which had large specific surface areas, was significantly weaker than that of the bulk material.

The PL show two emission peaks; one is having 389 nm could be attributed to band gap excitonic emission, which was blue shifted by the quantum confinement effect, and another one is having a 490 nm, due to the presence of oxygen defects. From the Fig. 4a-d, the increase in temperature with decrease in impurities and peak intensity. The number of sub peaks obtained from Gaussian peak function fitting of PL spectra shows the possible energy levels, the types of defects present in the samples and also their influence on the optical properties.

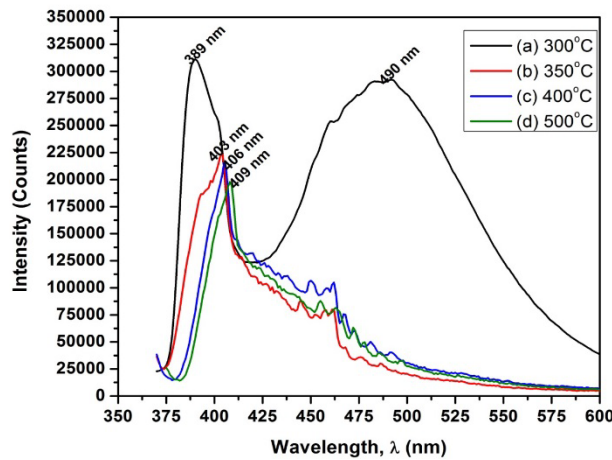


Fig. 4. Room temperature PL spectra of sprayed ZnO thin films.

3.4. UV-Vis-NIR analysis

The optical transmittance spectrum of ZnO films as shown in Fig. 5a-e. It is clearly indicate that Fig. 5a-e, the all ZnO films are found to be highly transparent between visible to near infrared region of the electromagnetic spectrum. The highly transmittance of 85-95% is observed from Fig.5a-e. The transmittance spectra clearly exhibit a shift in lower wavelength side due to the band gap absorption [30-35].

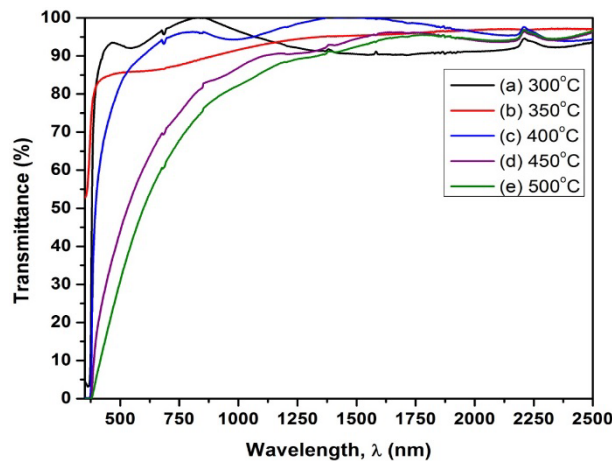


Fig. 5. Transmittance spectra of sprayed ZnO thin films.

The absorption coefficient (α) was calculated from the transmission data using the following Equation (5)

$$\alpha = \frac{\ln\left(\frac{1}{T}\right)}{t} \quad (5)$$

where, 'T' is the transmittance and 't' is the thickness of the film. The optical band gap of the films is determined using the following Equation (6)

$$\alpha h\nu = A(h\nu - E_g)^2 \quad (6)$$

where, A is the constant, $h\nu$ is the photon energy and E_g is the optical band gap energy. For $n=1/2$ the transition data provide the best linear curve in the band energy region, implying the direct transition.

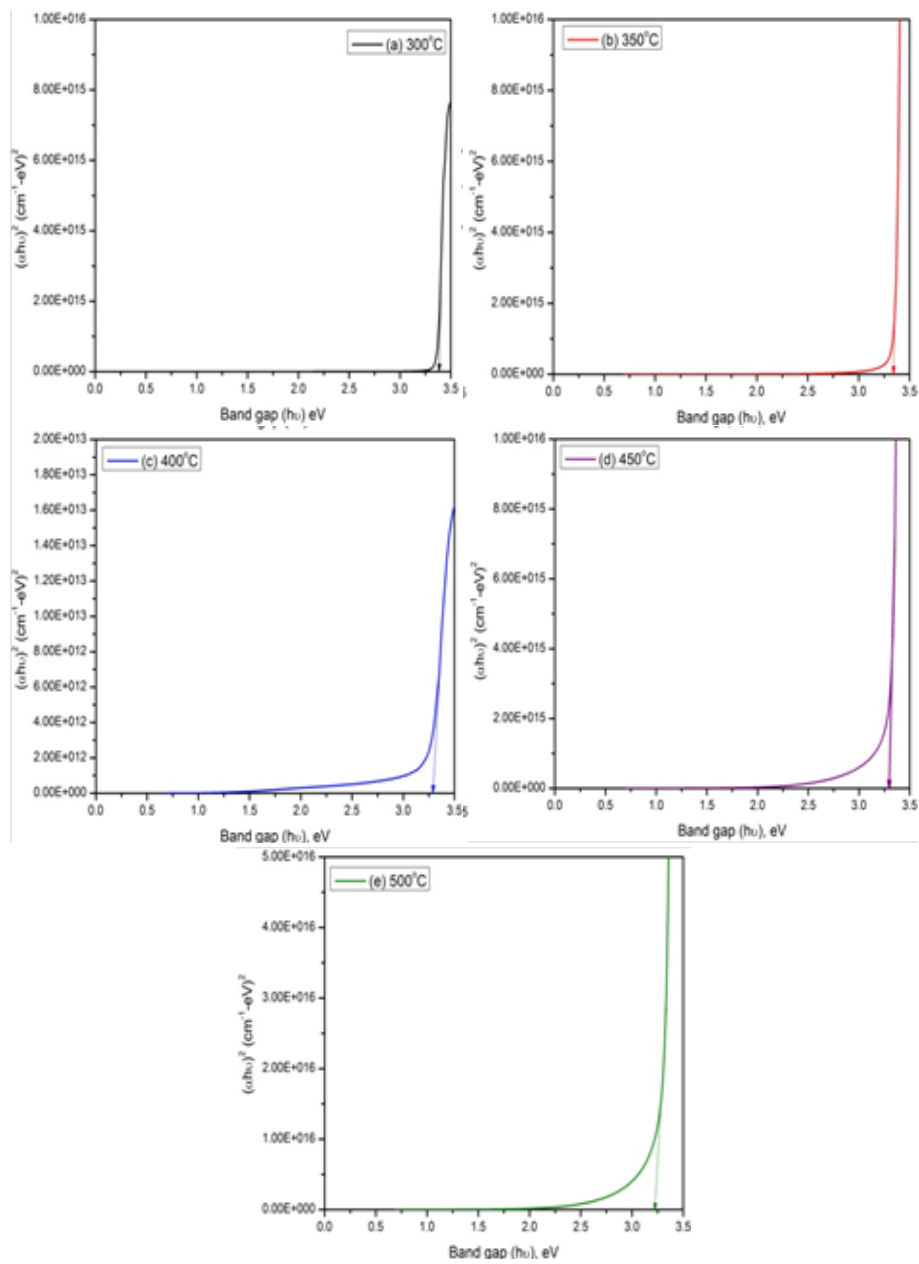


Fig. 6. Plots of $(ah\nu)^2$ vs $h\nu$ for nebulizer sprayed ZnO thin films.

Extrapolation of the straight line portion to zero absorption coefficient ($\alpha = 0$), gives the band gap energy. The plots of $(\alpha h\nu)$ versus $(h\nu)$ for ZnO films were deposited at different temperature from 300 to 500°C are shown in Fig. 6a-e. From Fig. 6a-e, the band gap energy values was found to be decreases from 3.37 eV to 3.2 eV with increase in temperature and which is supported by XRD and PL study. As temperature increases, the band gap energy decreases because the crystal lattice expands and the interatomic bonds are weakened. Weaker bonds means less energy is needed to break a bond and get an electron in the conduction band [36-39].

3.5. Impedance analysis

The complex Impedance spectra are generally plotted as Nyquist plot, i.e. imaginary component of impedance (Z'') versus real component (Z') as function of frequency. Bulk, grain boundary and electrode sample interface contributions to overall resistivity are determined by fitting of the experimental data to an equivalent circuit. The complex impedance spectra of ZnO films were deposited at 450 °C are investigated systematically in a as a function of temperature in the frequency range from 10 Hz to 1 MHz. From Fig.7a depicts the Nyquist plots of ZnO at various temperatures from 323 K to 573 K. It is observed that the Fig.7a, all plots of the semicircles are maximum is shifted to higher frequencies as increase in temperature. This is due to indicate that the electrical conductivity was thermally activated. To better analyse the impedance spectra, we assigned, to these spectra an equivalent ac circuit including connected parallel (R) and constant phase element (CPE). This circuit can be described by the earlier researchers [40-43]. The imaginary impedance versus frequency at various temperature is shown in Fig.7b. It is seen from the all plots that $-Z''$ increases with increase in frequency. The imaginary part of the impedance reaches a maximum value $-Z''_{max}$ which decreases with increase in temperature at the increase in relaxation frequency. The Variation of Z''/Z''_{max} versus f/f_{max} of the ZnO film at various temperatures are shown in Fig. 7c. From the Fig7 show that the same curve reveals that the relaxation dynamics processes were unaffected by temperature [20]. This result confirms that the relaxation process of charge carriers in ZnO film follow a similar process regardless of temperature.

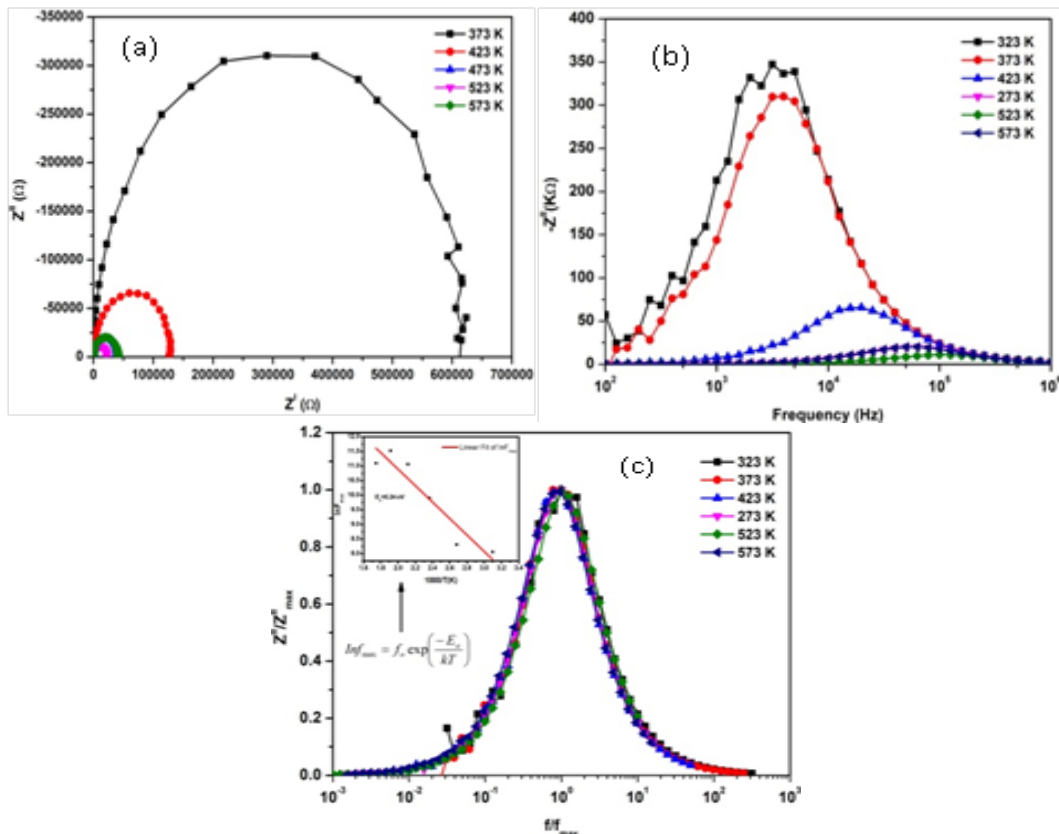


Fig. 7. (a) The Nyquist plot of ZnO films (b) Imaginary impedance versus frequency dependence (c) Variation of Z''/Z''_{max} versus f/f_{max} (c) Arrhenius plot of the Z'' is shown in the insert for ZnO thin films as a function of temperature.

This finding indicates that the frequency maximum followed Arrhenius behaviour. The calculated activation energy from Arrhenius Equation (7) is given below [44-45].

$$\ln f_{\max} = f_o \left[\frac{-E_a}{kT} \right] \quad (7)$$

where f_o is the pre exponential factor, E_a is a activation energy, k is the Boltzmann constant and T is the temperature in Kelvin. Insert Fig.7c represents the plot of $\ln(f_{\max})$ versus $(1000/T)$ giving a linear function. As temperature increases, molecules gain energy and move faster and faster. Therefore, the greater the temperature, the higher the probability that molecules will be moving with the necessary activation energy for a reaction to occur upon collision. The activation energy is found to be 0.24 eV. These indicates that the conduction mechanism may primarily due to the hopping of the electrons in ZnO film.

4. Conclusions

The Zinc Oxide (ZnO) thin films were deposited by simple and effective nebulizer spray pyrolysis method. From XRD analysis confirms a hexagonal crystal structure and which is found that the average crystallite size of the ZnO thin films with the temperature. The crystalline size was found to increases linearly with increase in temperature while decrease in dislocation density and microstrain. HR-SEM images reveals that the samples were highly uniform, homogeneous films consisting of nano-leaf and irregular spherical particles and average grain sizes are found to be ~50 nm at 500°C. The grain size increases with the increasing temperature. This is due to increasing the temperature leads to increase the crystallinity of the material and hence increases the number of crystallites. The PL spectra shows the two emission peaks, one is having at 389-409 nm which corresponds to band gap excitonic emission, and another is having located at 495-490 nm, due to the presence of defects. The UV-Vis-NIR spectra shows the all films are highly transparent in the visible region ~85-90 nm and optical band gap energy of the all films are found to be decreased from 3.37 eV to 3.2 eV with increase in temperature and which is supported by XRD and PL study. The impedance spectra of the ZnO thin films show the well-defined semicircular arc with its centre lying below the real axis at a particlular angle of depression, indicating a multi relaxation behaviour of ZnO films. Further, the arc observed in the low frequency is interpreted as due to the grain boundary effect. The real impedance exhibit activation energy at different temperature regions, indicating the presence of the donor carrier concentration and the impurity energy levels. In my conclusion, the ZnO film films are one of the most important conducting oxides and it is good solar cells, piezoelectric devices, gas sensors applications.

Acknowledgments

The authors are very much grateful to the Periyar University PG Extension Centre, Dharmapuri and University Grants Commission-South Eastern Regional Office (UGC-SERO), Hyderabad (India), for financial support under the project (No. MRP-4892/14 (SERO/UGC)) and Adhiyamaan College of Engineering (Autonomous), Hosur, Krishnagiri.

References

- [1] Ghariieb A. Ali, M. Emam-Ismail, M. El-Hagary, E.R. Shaaban, S.H. Moustafa, M.I. Amer, H. Shaban, *Optical Materials*, 119 (2021) 111312; <https://doi.org/10.1016/j.optmat.2021.111312>
- [2] V. Doni Pon, K.S. Joseph Wilson, K. Hariprasad, V. Ganesh, H. Elhosiny Ali, H. Algarni, I.S. Yahia, *Superlattices and Microstructures*, 151 (2021) 106790; <https://doi.org/10.1016/j.spmi.2020.106790>
- [3] Abdel-Galil, Mai S.A. Hussien, I.S. Yahia, *Optical Materials*, 114 (2021) 110894;

<https://doi.org/10.1016/j.optmat.2021.110894>

- [4] K. Siraj, Kashif Javaid, J.D. Pedarnig, M.A. Bodea, S. Naseem, *Journal of Alloys and Compounds*, 563 (2013) 280-284; <https://doi.org/10.1016/j.jallcom.2013.02.040>
- [5] E.S. Rajalekshmi, A.M.E. Raj, *Solid State Communications*, 338 (2021) 114479; <https://doi.org/10.1016/j.ssc.2021.114479>
- [6] R. Mariappan, V. Ponnuswamy, M. Ragavendar, *Materials Science in Semiconductor Processing*, 16 (2013) 1328-1335; <https://doi.org/10.1016/j.mssp.2012.10.012>
- [7] R. Mariappan, V. Ponnuswamy, R. Suresh, P. Suresh, A. Chandra Bose, M. Ragavendar, *Journal of Alloys and Compounds*, 582 (2014) 387-391; <https://doi.org/10.1016/j.jallcom.2013.08.048>
- [8] Taro Saito, Ariyuki Kato, Kanji Yasui, *Journal of Crystal Growth*, 570 (2021) 126206; <https://doi.org/10.1016/j.jcrysgro.2021.126206>
- [9] Tianlei Ma, *Materials Science in Semiconductor Processing*, 121 (2021) 105413; <https://doi.org/10.1016/j.mssp.2020.105413>
- [10] P. Soundarrajan, K. Sankarasubramanian, T. Logu, K. Sethuraman, Arunava Gupta, S.M. Senthil Kumar, K. Jeganathan, K. Ramamurthi, *Physica E: Low-dimensional Systems and Nanostructures*, 106 (2018) 50-56; <https://doi.org/10.1016/j.physe.2018.10.010>
- [11] Nguyen Thanh Son, Jin-Seo Noh, Sungho Park, *Applied Surface Science*, 379 (2016) 440-445; <https://doi.org/10.1016/j.apsusc.2016.04.107>
- [12] Y.-J. Lin, H.-C. Chang, C. Y. Chuang, P.-E. Lu, J.-S. Huang, *Journal of Alloys and Compounds*, 890 (2022) 161796; <https://doi.org/10.1016/j.jallcom.2021.161796>
- [13] Z. R. Khan, A. S. Alshammari, M. Bouzidi, M. Shkir, D. K. Shukla, *Chemistry Communications*, 132 (2021) 108812; <https://doi.org/10.1016/j.inoche.2021.108812>
- [14] Hassan Ahmoum, Guojian Li, Sarra Belakry, Mourad Boughrara, Mohd Sukor Suait, Mohamed Kerouad, Qiang Wang, *Materials Science in Semiconductor Processing*, 123(2021) 105530; <https://doi.org/10.1016/j.mssp.2020.105530>
- [15] N.H. Sheeba, Sunil C. Vattappalam, G.S. Okram, Vikash Sharma, P.V. Sreenivasan, Sunny Mathew, Rachel Reena Philip, *Materials Research Bulletin* 93 (2017) 130-137. S0025540816306304; <https://doi.org/10.1016/j.materresbull.2017.04.021>
- [16] M. Shaheera, K.G. Girija, Manmeet Kaur, V. Geetha, A.K. Debnath, R.K. Vatsa, K.P. Muthe, S.C. Gadkari, *Chemical Physics Letters*, 758 (2020) 137951; <https://doi.org/10.1016/j.cplett.2020.137951>
- [17] Mirabbos Hojamberdiev, Ronald Vargas, Vijendra Singh Bhati, Daniel Torres, Zukhra C. Kadirova, Mahesh Kumar, *Journal of Electroanalytical Chemistry*, 882 (2021) 115009; <https://doi.org/10.1016/j.jelechem.2021.115009>
- [18] S. Jessadaluk, N. Khemasiri, P. Rattanawarinchai, N. Kayunkid, S. Rahong, A. Rangkasikorn, J. Nukeaw, *Optical Materials*, 120 (2021) 111461; <https://doi.org/10.1016/j.optmat.2021.111461>
- [19] Vinod Kumar, O.M. Ntwaeaborwa, H.C. Swart, *Physica B: Condensed Matter*, 576 (2020) 411713; <https://doi.org/10.1016/j.physb.2019.411713>
- [20] Dipak A. Tonpe, Ketan P. Gattu, Vishnu V. Kutwade, Makrand E. Sonawane, Avinash S. Dive, Ramphal Sharma, *Journal of Materials Science: Materials in Electronics*, (2019); <https://doi.org/10.1007/s10854-019-01976-9>
- [21] Rayees Ahmad Zargar, Manju Arora, Riyaz Ahmed Bhat, *Applied Physics A*, 124(1)(2018) 36-45; <https://doi.org/10.1007/s00339-017-1457-5>
- [22] Yogendra Kumar, Amit Kumar Rana, Prateek Bhojane, Manojit Pusty, Vivas Bagwe, Somaditya Sen, Parasharam M Shirage, *Materials Research Express*, 2(10)(2015) 105017; <https://doi.org/10.1088/2053-1591/2/10/105017>
- [23] J. E. Ramos, M. Montero-Munoz, J. A. H. Coaquira, J. E. Rodriguez-Paez, *Mn- Journal of Low Temperature Physics*, 179(1-2)(2015) 42-47; <https://doi.org/10.1007/s10909-014-1246-x>
- [24] Punam Murkute, Hemant Ghadi, Sheshadri Sreedhara, Subhananda Chakrabarti, *Superlattices and Microstructures*, 136 (2019), 106310; <https://doi.org/10.1016/j.spmi.2019.106310>

- [25] B. KaniAmuthan, S. Vinoth, Vaithinathan Karthikeyan, Vellaisamy A.L.Roy, P. Thilakan, *Ceramics International*, 45 (2019) 24324-24330; <https://doi.org/10.1016/j.ceramint.2019.08.147>
- [26] E. Hasabeldaim, O.M. Ntwaeaborwa, R.E. Kroon, H.C. Swart, *Journal of Molecular Structure*, 1192 (2019)105-114; <https://doi.org/10.1016/j.molstruc.2019.04.128>
- [27] E. Musavi, M. Khanlary, Z. Khakpour, *Journal of Luminescence*, 216(2019), 116696; <https://doi.org/10.1016/j.jlumin.2019.116696>
- [28] E.H.H. Hasabeldaim, O.M. Ntwaeaborwa, R.E. Kroon, E. Coetsee, H.C. Swart, *Vacuum*, 169 (2019)108889; <https://doi.org/10.1016/j.vacuum.2019.108889>
- [29] Shahid Atiq, M. Tamoor Ansar, Ali Hassan, S. Kumail Abbas, Taswar Iqbal, Mushtaq Aslam, M. Javaid Iqbal, Asif Mahmood, *Superlattices and Microstructures*, 144 (2020) 106576; <https://doi.org/10.1016/j.spmi.2020.106576>
- [30] Mursal, Irhamni, Bukhari, Zulkarnain Jalil, *Journal of Physics: Conference Series*, 1116 (2018) 032020; <https://doi.org/10.1088/1742-6596/1116/3/032020>
- [31] A. Bedia, F. Bedia, M. Aillerie, N. Maloufi, B. Benyoucef, *Solar Cell*, 74 (2015) 529-538; <https://doi.org/10.1016/j.egypro.2015.07.740>
- [32] A.M. Alsaad, Al-Bataineh, M. Qais, A.A. Ahmad, Zaid Albataineh, Ahmad Telfah, *Optik*, 211(2020) 164641; <https://doi.org/10.1016/j.ijleo.2020.164641>
- [33] Lirong Sun, John T.Grant, John G.Jones, Neil R. Murphy, *Optical Materials*, 84(2018)146-157; <https://doi.org/10.1016/j.optmat.2018.06.024>
- [34] Nishant Kumar, Anu Katiyar, Anchal Srivastava, *Materials Today: Proceedings*, 5(2018) 9089-9093; <https://doi.org/10.1016/j.matpr.2017.10.025>
- [35] Won Mok Kim, Jin Soo Kim, Jeung-hyun Jeong, Jong-Keuk Park, Young-Jun Baik, Tae-Yeon Seong, *Thin Solid Films*, 531(2013) 430-435; <https://doi.org/10.1016/j.tsf.2013.01.078>
- [36] N. Kumar, A. Srivastava, *Opto-Electronics Review*, 26(2018) 1-10; <https://doi.org/10.1016/j.opelre.2017.11.001>
- [37] Asim Jilani, M.Sh. Abdel-wahab, H.Y. Zahran, I.S. Yahia, Attieh A. Al-Ghamdi, Ahmed Alshahrie, A.M. El-Naggar, *Optik*, 164 (2018) 143-154; <https://doi.org/10.1016/j.ijleo.2018.02.073>
- [38] Won Mok Kim, Jin Soo Kim, Jeung-hyun Jeong, Jong-Keuk Park, Young-Jun Baik, Tae-Yeon Seong, *Thin Solid Films*, 531(2013) 430-435; <https://doi.org/10.1016/j.tsf.2013.01.078>
- [39] Y. Chen, X.L. Xu, G.H. Zhang, H. Xue, S.Y. Ma, *Physica E* 42(2010) 1713-1716; <https://doi.org/10.1016/j.physe.2010.01.029>
- [40] Mohamed Salah, Samir Azizi, Abdelwaheb Boukhachem, Chokri Khaldi, Mosbah Amlouk, Jilani Lamloumi, *Applied Physics A*, 125(9) (2019) 615-636; <https://doi.org/10.1007/s00339-019-2911-3>
- [41] Sevcik Jakub, Urbanek Pavel, Skoda David, Jamatia Thaiskang, Nadazdy Vojtech, Urbanek Michal, Antos Jan, Munster Lukas, Kuritka Ivo, *Materials & Design*, 205 (2021)109738; <https://doi.org/10.1016/j.matdes.2021.109738>
- [42] Luciano D. Sappia, Matias R.Trujillo, Israel Lorite, Rossana E. Madrid,, Monica Tirado, David Comedi, Pablo Esquinazi, *Materials Science and Engineering: B*, 200 (2015)124-131; <https://doi.org/10.1016/j.mseb.2015.06.005>
- [43] Israel Lorite, Laura Villaseca, Pilar Díaz-Carrasco, Mercedes Gabas, Jose Luis Costa-Krämer, *Thin Solid Films*, 548 (2013) 657-660; <https://doi.org/10.1016/j.tsf.2013.09.077>
- [44] Nanda Shakti, Tapendu Mandal, Asit Prakash, Gangadhar Purohit, *Surfaces and Interfaces*, 9 (2017) 228-232; <https://doi.org/10.1016/j.surfin.2017.10.004>
- [45] E.S. Kadir, R.N. Gayen, R. Paul, S. Biswas, *Journal of Alloys and Compounds*, 843 (2020), 155974; <https://doi.org/10.1016/j.jallcom.2020.155974>